BIOMEDICINE

3D bioprinting of collagen to rebuild components of the human heart

A. Lee[1]*, A. R. Hudson[1]*, D. J. Shiwarski[1], J. W. Tashman[1], T. J. Hinton[1], S. Yerneni[1], J. M. Bliley[1], P. G. Campbell[1,2], A. W. Feinberg[1,3]†

Collagen is the primary component of the extracellular matrix in the human body. It has proved challenging to fabricate collagen scaffolds capable of replicating the structure and function of tissues and organs. We present a method to 3D-bioprint collagen using freeform reversible embedding of suspended hydrogels (FRESH) to engineer components of the human heart at various scales, from capillaries to the full organ. Control of pH-driven gelation provides 20-micrometer filament resolution, a porous microstructure that enables rapid cellular infiltration and microvascularization, and mechanical strength for fabrication and perfusion of multiscale vasculature and tri-leaflet valves. We found that FRESH 3D-bioprinted hearts accurately reproduce patient-specific anatomical structure as determined by micro–computed tomography. Cardiac ventricles printed with human cardiomyocytes showed synchronized contractions, directional action potential propagation, and wall thickening up to 14% during peak systole.

For biofabrication, the goal is to engineer tissue scaffolds to treat diseases for which there are limited options, such as end-stage organ failure. Three-dimensional (3D) bioprinting has achieved important milestones including microphysiological devices (*1*), patterned tissues (*2*), perfusable vascular-like networks (*3*–*5*), and implantable scaffolds (*6*). However, direct printing of living cells and soft biomaterials such as extracellular matrix (ECM) proteins has proved difficult (*7*). A key obstacle is the problem of supporting these soft and dynamic biological materials during the printing process to achieve the resolution and fidelity required to recreate complex 3D structure and function. Recently, Dvir and colleagues 3D-printed a decellularized ECM hydrogel into a heart-like model and showed that human cardiomyocytes and endothelial cells could be integrated into the print and were present as spherical nonaligned cells after 1 day in culture (*8*). However, no further structural or functional analysis was performed.

We report the ability to directly 3D-bioprint collagen with precise control of composition and microstructure to engineer tissue components of the human heart at multiple length scales. Collagen is an ideal material for biofabrication because of its critical role in the ECM, where it provides mechanical strength, enables structural organization of cell and tissue compartments, and serves as a depot for cell adhesion and signaling molecules (*9*). However, it is difficult to 3D-bioprint complex scaffolds using collagen in its native unmodified form because gelation is typically achieved using thermally driven self-assembly, which is difficult to control. Researchers have used approaches including

[1]Department of Biomedical Engineering, Carnegie Mellon University, Pittsburgh, PA 15213, USA. [2]Engineering Research Accelerator, Carnegie Mellon University, Pittsburgh, PA 15213, USA. [3]Department of Materials Science and Engineering, Carnegie Mellon University, Pittsburgh, PA 15213, USA.
*These authors contributed equally to this work.
†Corresponding author. Email: feinberg@andrew.cmu.edu

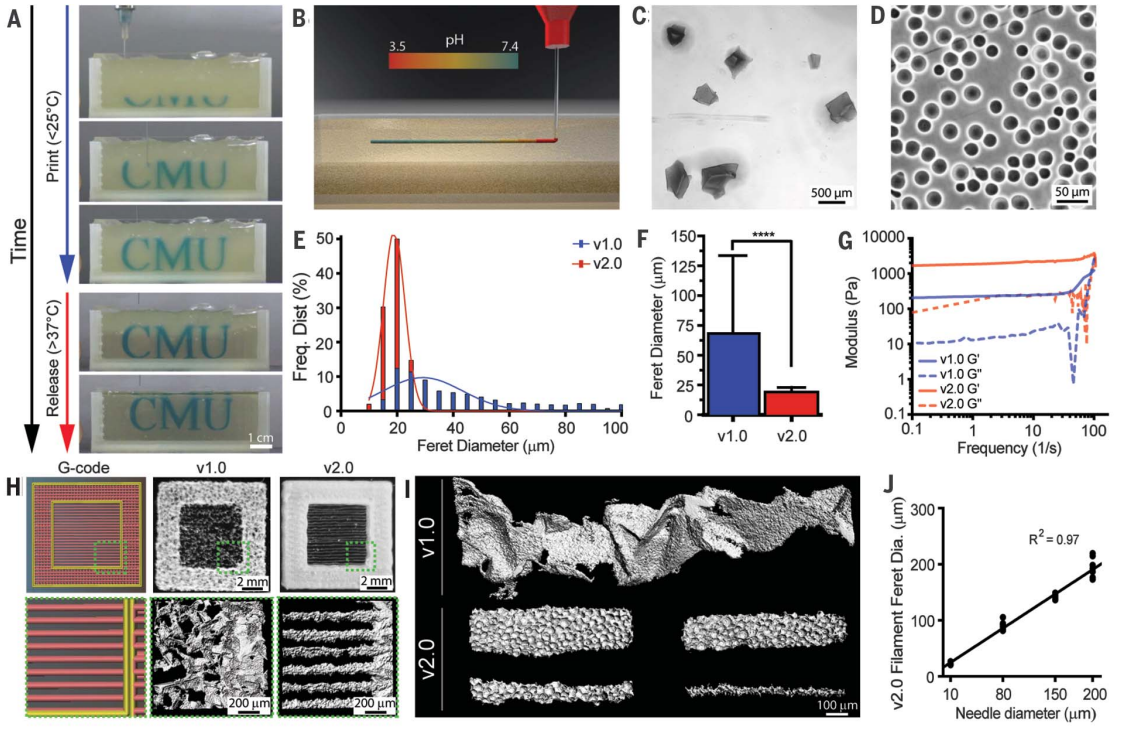

Fig. 1. High-resolution 3D bioprinting of collagen using FRESH v2.0. (**A**) Time-lapse sequence of 3D bioprinting of the letters "CMU" using FRESH v2.0. (**B**) Schematic of acidified collagen solution extruded into the FRESH support bath buffered to pH 7.4, where rapid neutralization causes gelation and formation of a collagen filament. (**C** and **D**) Representative images of the gelatin microparticles in the support bath for (C) FRESH v1.0 and (D) v2.0, showing the decrease in size and polydispersity. (**E**) Histogram of Feret diameter distribution for gelatin microparticles in FRESH v1.0 (blue) and v2.0 (red). (**F**) Mean Feret diameter of gelatin microparticles for FRESH v1.0 and v2.0 [$N > 1200$, data are means ± SD, ****$P < 0.0001$ (Student t test)]. (**G**) Storage (G′) and loss (G″) moduli for FRESH v1.0 and v2.0 support baths showing yield stress fluid behavior. (**H**) A "window-frame" print construct with single filaments across the middle, comparing G-code (left), FRESH v1.0 (center), and FRESH v2.0 (right). (**I**) Single filaments of collagen showing the variability of the smallest diameter (~250 µm) that can be printed using FRESH v1.0 (top) compared to relatively smooth filaments 20 to 200 µm in diameter using FRESH v2.0 (bottom). (**J**) Collagen filament Feret diameter as a function of extrusion needle internal diameter for FRESH v2.0, showing a linear relationship.

chemically modifying collagen into an ultraviolet (UV)–cross-linkable form (*10*), adjusting pH, temperature, and collagen concentration to control gelation and print fidelity (*11*, *12*), and/or denaturing it into gelatin (*13*) to make it thermoreversible. However, these hydrogels are typically soft and tend to sag, and they are difficult to print with high fidelity beyond a few layers in height. Instead, we developed an approach that uses rapid pH change to drive collagen self-assembly within a buffered support material, enabling us to (i) use chemically unmodified collagen as a bio-ink, (ii) enhance mechanical properties by using high collagen concentrations of 12 to 24 mg/ml, and (iii) create complex structural and functional tissue architectures. To accomplish this, we developed a substantially improved second generation of the freeform reversible embedding of suspended hydrogels (FRESH v2.0) 3D-bioprinting technique used in combination with our custom-designed open-source hardware platforms (fig. S1) (*14*, *15*). FRESH works by extruding bio-inks within a thermoreversible support bath composed of a gelatin microparticle slurry that provides support during printing and is subsequently melted away at 37°C (Fig. 1, A and B, and movie S1) (*16*).

The original version of the FRESH support bath, termed FRESH v1.0, consisted of irregularly shaped microparticles with a mean diameter of ~65 μm created by mechanical blending of a large gelatin block (Fig. 1C) (*16*). In FRESH v2.0, we developed a coacervation approach to generate gelatin microparticles with (i) uniform spherical morphology (Fig. 1D), (ii) reduced polydispersity (Fig. 1E), (iii) decreased particle diameter of ~25 μm (Fig. 1F), and (iv) tunable storage modulus and yield stress (Fig. 1G and fig. S2). FRESH v2.0 improves resolution with the ability to precisely generate collagen filaments and accurately reproduce complex G-code, as shown with a window-frame calibration print (Fig. 1H). Using FRESH v1.0, the smallest collagen filament reliably printed was ~250 μm in mean diameter, with highly variable morphology due to the relatively large and polydisperse gelatin microparticles (Fig. 1I). In contrast, FRESH v2.0 improves the resolution by an order of magnitude, with collagen filaments reliably printed from 200 μm down to 20 μm in diameter (Fig. 1, I and J). Filament morphology from solid-like to highly porous was controlled by tuning the collagen gelation rate using salt concentration and buffering capacity of the gelatin support bath (fig. S3). A pH 7.4 support bath with 50 mM HEPES was the optimal balance between individual strand resolution and strand-to-strand adhesion and was versatile, enabling FRESH printing of multiple bio-inks with orthogonal gelation mechanisms including collagen-based inks, alginate, fibrinogen, and methacrylated hyaluronic acid in the same print by adding $CaCl_2$, thrombin, and UV light exposure (fig. S4) (*15*).

We first focused on FRESH-printing a simplified model of a small coronary artery–scale linear tube from collagen type I for perfusion with a custom-designed pulsatile perfusion system (Fig. 2A and fig. S5). The linear tube had an inner diameter of 1.4 mm (fig. S6A) and a wall thickness of ~300 μm (fig. S6B), and was patent and manifold as determined by dextran perfusion (fig. S6, C to E, and movie S2) (*15*). C2C12 cells within a collagen gel were cast around the printed collagen tube to evaluate the ability to support a volumetric tissue. The static nonperfused controls showed minimal compaction over 5 days (Fig. 2B), and a cross section revealed dead

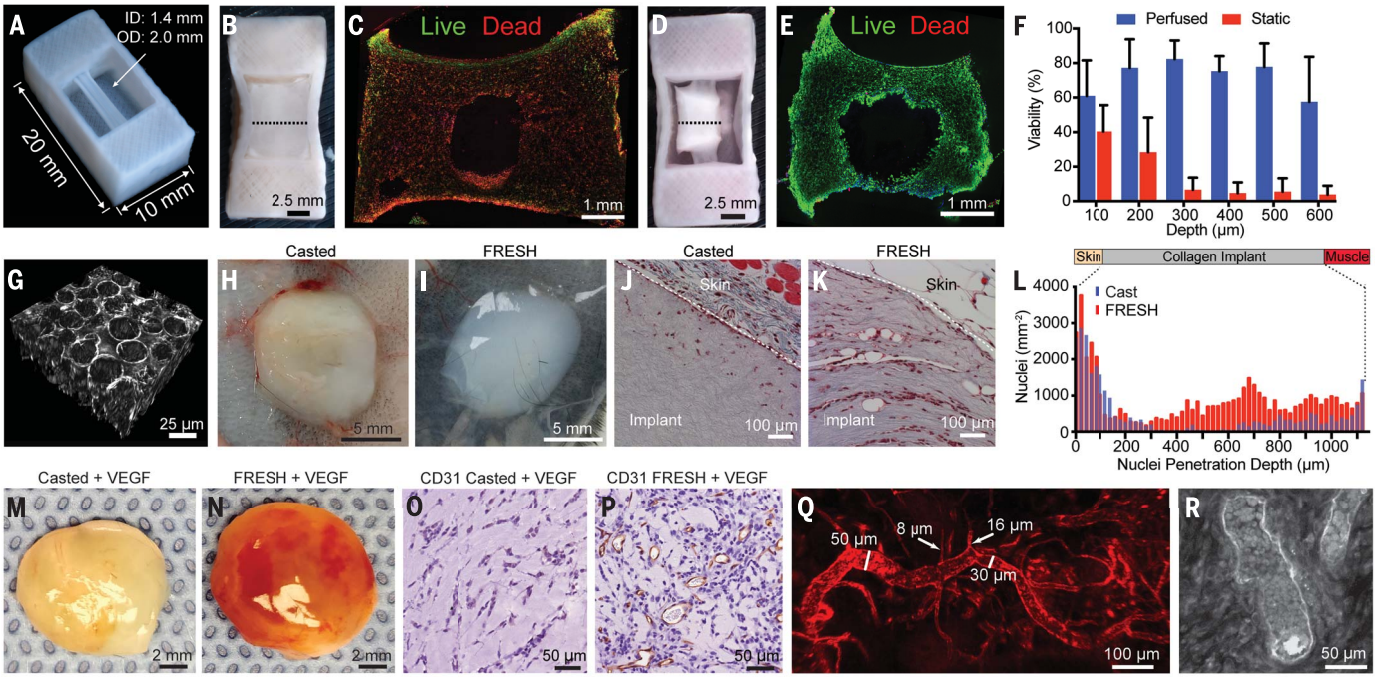

Fig. 2. FRESH 3D bioprinting of perfusable collagen vessels and microporous collagen scaffolds that promote in vivo microvascularization. (**A**) FRESH-printed collagen tube construct. (**B**) C2C12 cell and collagen gel mixture cast around the collagen tube and static-cultured for 5 days. (**C**) Cross section of the tissue from (B) stained for live (green) and dead (red) cells. (**D**) C2C12 cell and collagen gel mixture cast around the collagen tube and perfused for 5 days. (**E**) Cross section of the tissue from (D) stained for live and dead cells. (**F**) Percent cell viability as a function of depth from the top surface of the tissues from the static and perfused collagen tube constructs [$N = 3$, data are means ± SD, $^*P < 0.05$ (two-way ANOVA followed by Bonferroni multiple-comparisons posttest)]. (**G**) Multiphoton imaging showing microscale porosity in FRESH-printed collagen constructs after removal of the gelatin microparticle support bath. (**H** and **I**) Collagen constructs cast (H) and FRESH-printed (I) without VEGF 7 days after subcutaneous implantation. (**J** and **K**) Masson's trichrome staining to visualize cells (red) and collagen (blue) in cast (J) and FRESH-printed (K) collagen disks after 7 days of subcutaneous implantation. (**L**) Cell density after implantation as a function of depth for the cast and FRESH-printed collagen disks. (**M** and **N**) Collagen constructs cast (M) and FRESH-printed (N) with VEGF (100 ng/ml) 10 days after subcutaneous implantation. (**O** and **P**) CD31 staining (brown) and cells (blue) of cast (O) and FRESH-printed (P) collagen disks doped with VEGF (100 ng/ml) after 10 days of subcutaneous implantation. (**Q**) Host vascular infiltration of vessels (diameter 8 to 50 μm) in the FRESH-printed collagen disk labeled by lectin tail vein injection (red). (**R**) Multiphoton image 70 μm into the FRESH-printed construct, showing red blood cells within the lumen of the microvasculature.

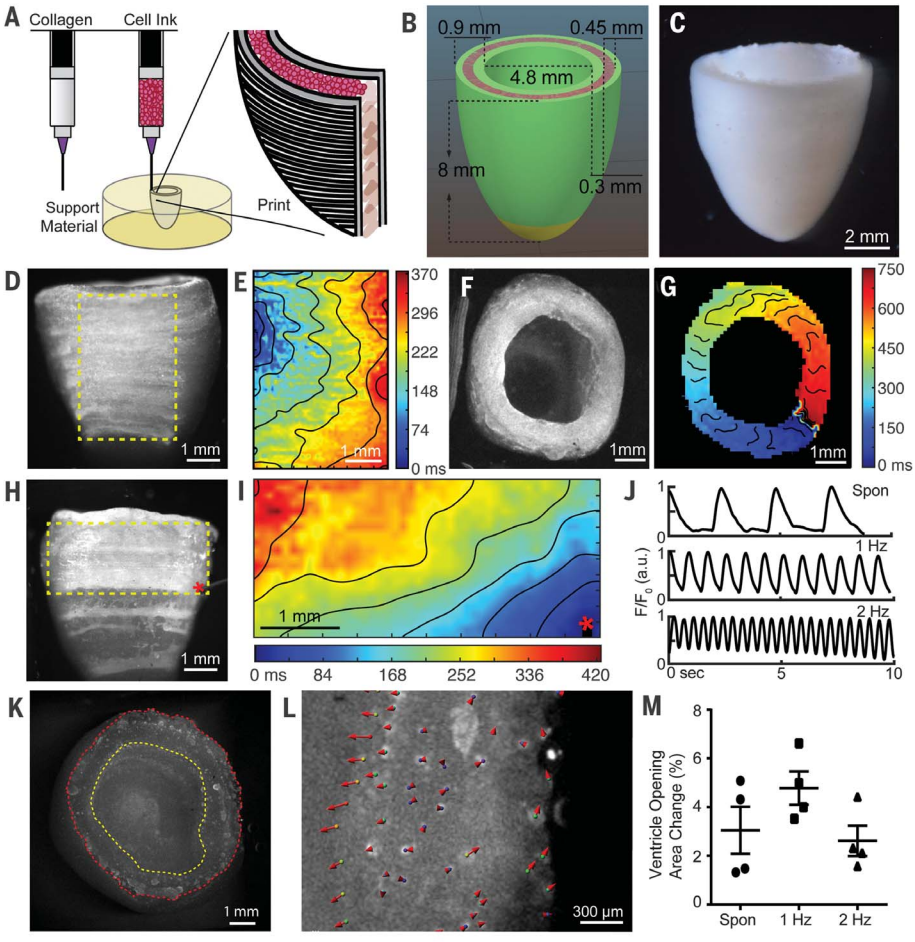

Fig. 3. Contractile FRESH 3D-bioprinted human cardiac ventricle model. (**A**) Schematic of dual-material FRESH printing using a collagen ink and a high-concentration cell ink. (**B**) Ventricle model with a central section of cardiac cells (pink), internal and external collagen shells (green), and a collagen-only section (yellow). (**C**) Micrograph of FRESH-printed ventricle. (**D**) Side view of FRESH-printed ventricle stained with calcium-sensitive dye showing uniform cell distribution. (**E**) Calcium mapping of the subregion [yellow box in (D)] showing spontaneous, directional calcium wave propagation with conduction velocity of 1.97 cm/s. (**F**) Top view of FRESH-printed ventricle stained with calcium-sensitive dye. (**G**) Calcium mapping showing spontaneous circular calcium wave propagation around the ventricle with conduction velocity of 1.31 cm/s. (**H**) Point stimulation of FRESH-printed ventricle stained with calcium-sensitive dye (red asterisk indicates electrode location). (**I**) Calcium mapping of the subregion [yellow box in (H)] showing anisotropic calcium wave propagation with longitudinal conduction velocity of 2.0 cm/s. (**J**) Calcium transient traces during spontaneous contractions (top), 1-Hz field stimulation (middle), and 2-Hz field stimulation (bottom). Calcium fluorescence intensity (F) is normalized by dividing by baseline fluorescence intensity (F_0). (**K**) Top-down image of the FRESH-printed ventricle with inner (yellow) and outer (red) walls outlined. (**L**) A subregion of the ventricular wall analyzed for displacement during 1-Hz field stimulation, showing inner and outer wall motion; magnitude and direction are indicated by red arrows. (**M**) Cross-sectional area of the ventricle interior chamber at peak systole (N = 4, data are means ± SD).

cells throughout the interior volume with a layer of viable cells only at the surface (Fig. 2C). In contrast, after active perfusion for 5 days, C2C12 cells compacted the collagen gel around the collagen tube (Fig. 2D), demonstrating viability and active remodeling of the gel through cell-driven compaction. The cross section showed cells alive throughout the entire volume (Fig. 2E), and quantitative analysis using LIVE/DEAD staining confirmed high viability within the perfused vascular construct (Fig. 2F). Others have 3D-bioprinted vasculature by casting cell-laden hydrogels around fugitive filaments, which become the vessel lumens (*4*, *5*). In comparison, we directly print collagen to form the walls of a functional vascular channel, serving as the foundation for engineering more complex architectures.

Engineering smaller-scale vasculature, especially on the order of capillaries (5 to 10 μm in diameter), has been a challenge for extrusion-based 3D bioprinting because this is far below common needle diameters. However, at this length scale, endothelial and perivascular cells can self-assemble vascular networks through angiogenesis (*17*). We reasoned that the gelatin microparticles in the FRESH v2.0 support bath could be incorporated into the 3D-bioprinted collagen to create a porous microstructure, specifically because pores on the order of 30 μm in diameter have been shown to promote cell infiltration and microvascularization (*18*). FRESH v2.0–printed constructs contained micropores ~25 μm in diameter resulting from the melting and removal of the gelatin microparticles purposely entrapped during the printing process (Fig. 2G and movie S3). Collagen disks 5 mm thick and 10 mm in diameter were cast in a mold or printed and implanted in an in vivo murine subcutaneous vascularization model (Fig. 2, H and I, and fig. S7, A and B) to observe cellular infiltration. After implantation for 3 and 7 days, collagen disks were extracted and assessed for gross morphology, cellularization, and collagen structure (fig. S7, C to E). The solid-cast collagen showed minimal cell infiltration (Fig. 2J), whereas the printed collagen had extensive cell infiltration and collagen remodeling (Fig. 2K). Quantitative analysis revealed that cells infiltrated throughout the printed collagen disk within 3 days (Fig. 2L and fig. S8) and that the number of cells in the constructs was significantly greater for the printed collagen at 3 and 7 days compared to cast control [N = 6, P < 0.0001, two-way analysis of variance (ANOVA)] (*15*).

To promote vascularization, we incorporated fibronectin and the proangiogenic molecule recombinant vascular endothelial growth factor (VEGF) into our collagen bio-ink (*19*). Collagen disks that were FRESH-printed with VEGF and extracted after 10 days in vivo showed enhanced vascularization relative to cast controls (Fig. 2, M and N). By histology, the addition of VEGF to the cast collagen increased cell infiltration without promoting microvascularization (Fig. 2O and fig. S9). In contrast, the addition of VEGF to the printed collagen resulted in widespread vascularization, with CD31-positive vessels and red blood cells visible within the lumens (Fig. 2P). Tail vein injection of fluorescent lectin confirmed an extensive host-derived vascular network with vessels ranging from 8 to 50 μm in diameter throughout the printed collagen disk (Fig. 2Q, fig. S10, and movie S4). Multiphoton microscopy enabled deeper imaging into the printed constructs and showed vessels containing red blood cells at depths of at least 200 μm (Fig. 2R and movie S5).

We next FRESH-printed a model of the left ventricle of the heart using human stem cell–derived cardiomyocytes. We used a dual-material printing strategy with collagen bio-ink as the structural component in combination with a high-density cell bio-ink (Fig. 3A) (*15*). A test print design (fig. S11A) verified that the collagen pH was neutralized quickly enough to maintain ~96% post-printing viability by LIVE/DEAD staining (fig. S11B). The ventricle was designed as

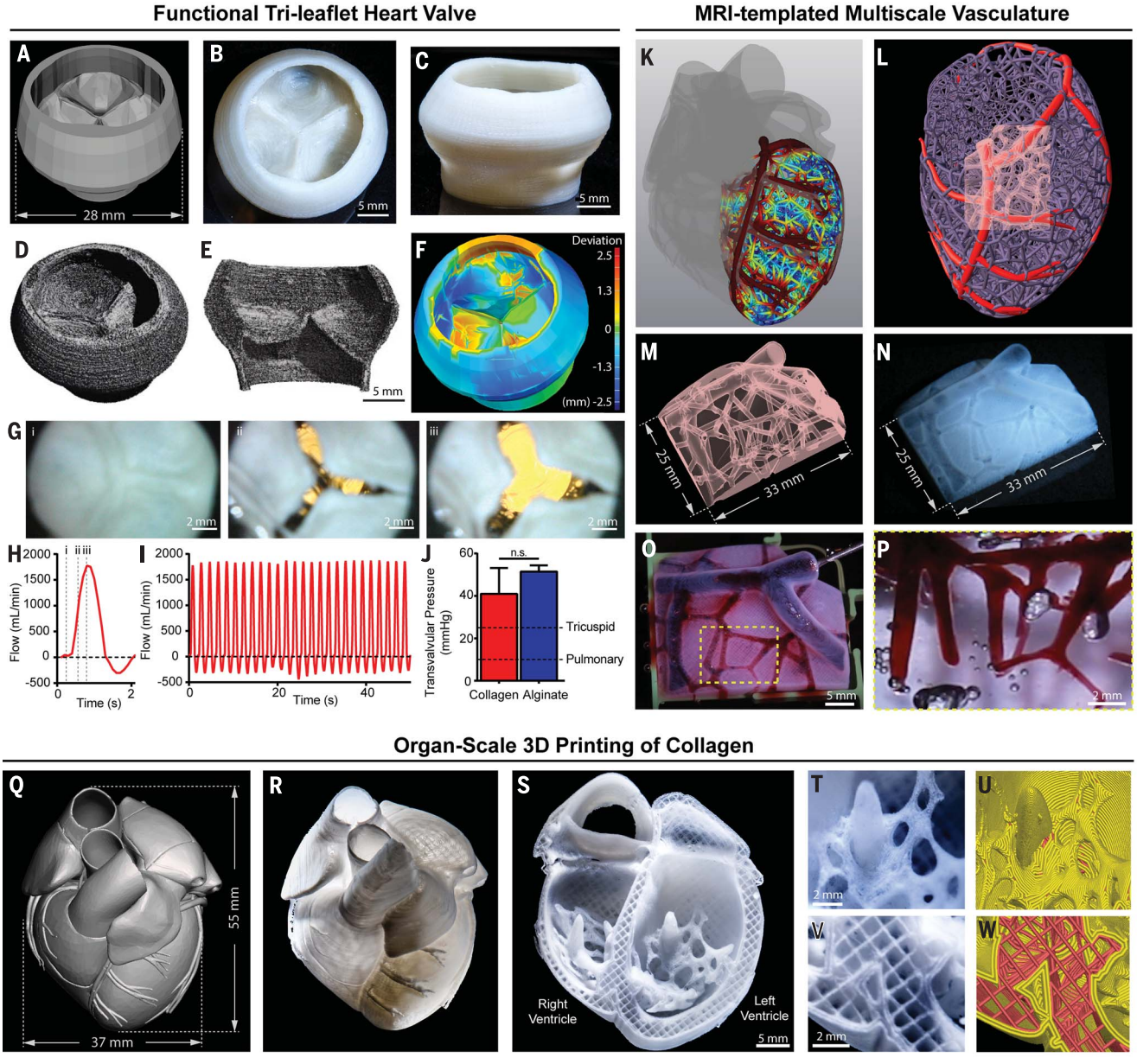

Fig. 4. Organ-scale FRESH 3D bioprinting of tri-leaflet heart valve, multiscale vasculature, and neonatal-scale human heart. (**A**) Tri-leaflet heart valve 3D model at adult human scale. (**B** and **C**) Top and side views of FRESH-printed collagen heart valve with barium sulfate added for x-ray contrast. (**D**) μCT reconstruction showing the full printed valve. (**E**) Lateral cross section of the wall and leaflets. (**F**) Quantitative gauging of the μCT 3D surface compared to the 3D model, showing average overprinting of +0.55 mm and underprinting of −0.80 mm. (**G**) Sequence of valve opening under pulsatile flow over ~1 s. (**H**) Doppler flow velocimetry of a single cycle: (i) closed, (ii) half-open, and (iii) open. (**I**) Same as (H) over multiple cycles. (**J**) Maximum transvalvular pressure of printed alginate and collagen valves compared to operating pressure for native valves [$N = 3$, data are means ± SD, n.s. indicates $P > 0.05$ (Student t test)]. (**K**) MRI-derived 3D human heart model (gray) with computationally derived multiscale vascular network shown for the the left ventricle. The left anterior descending coronary artery (red) is the template to guide the formation of smaller-scale vessels, which decrease in diameter according to distance from the coronary artery (red to blue). (**L**) Left ventricle with the left anterior descending artery (red), computationally generated vasculature (purple), and subregion of interest (pink). (**M**) Transparent subregion showing 3D structure of the vascular network. (**N**) The subregion FRESH-bioprinted with collagen, showing reproduction of the vascular network. (**O**) Perfusion of the vascular network with glycerol (red) through the coronary artery, showing interconnectivity. (**P**) Collagen was optically cleared and perfused with glycerol (red), showing perfusion down to vessels ~100 μm in diameter. (**Q**) MRI-derived 3D human heart scaled to neonatal size. (**R**) FRESH-printed collagen heart. (**S**) Cross-sectional view of the collagen heart, showing left and right ventricles and interior structures. (**T** and **U**) High-fidelity image of the trabeculae in the left ventricle (T) showing reproduction of the complex anatomical structure from the G-code (U). (**V** and **W**) High-fidelity image of the septal wall between ventricles (V) showing reproduction of the square-lattice infill from the G-code (W).

an ellipsoidal shell (Fig. 3B) with inner and outer walls of collagen and a central core region containing human embryonic stem cell–derived cardiomyocytes (hESC-CMs) and 2% cardiac fibroblasts (fig. S11, C to H). Ventricles were printed and cultured for up to 28 days, during which the collagen inner and outer walls provided sufficient structural integrity to maintain their intended geometry (Fig. 3C). After 4 days, the ventricles visibly contracted, and after 7 days they became synchronous with a dense layer of interconnected and striated hESC-CMs, as confirmed by immunofluorescent staining of sarcomeric α-actinin–positive myofibrils (fig. S11, I to K). Calcium imaging revealed contracting hESC-CMs throughout the entire printed ventricles, with directional wave propagation in the direction of the printed hESC-CMs observed from the side (Fig. 3, D and E) and top (Fig. 3, F and G) during spontaneous contractions in multiple ventricles (N = 3) (movie S6). Point stimulation enabled visualization of anisotropic calcium wave propagation with longitudinal conduction velocity of ~2 cm/s and a longitudinal-to-transverse anisotropy ratio of ~1.5 (Fig. 3, H and I). The ventricles had a baseline spontaneous beat rate of ~0.5 Hz and could be captured and paced at 1 and 2 Hz by means of field stimulation (Fig. 3J). We imaged the ventricles top-down to quantify motion of the inner and outer walls (Fig. 3K). Wall thickening is a hallmark of normal ventricular contraction. The printed ventricle expanded both inward and outward during a contraction, as determined by particle tracking to map the deformation field (Fig. 3L). The decrease in cross-sectional area of the interior chamber during peak systole showed a maximum of ~5% at 1-Hz pacing (N = 4) (Fig. 3M and movie S6). We also observed electrophysiologic behavior associated with arrhythmogenic disease states, including multiple propagating waves (fig. S12, A and B) and pinned rotors (fig. S12, C and D).

To demonstrate the mechanical integrity and function of collagen constructs at adult human scale, we printed a tri-leaflet heart valve 28 mm in diameter (Fig. 4A). We first prototyped the valve using alginate, a material previously used to build valve models (*20*), and then printed a collagen valve and improved the mechanical properties by adapting published fixation protocols for decellularized porcine heart valves (fig. S13A) (*15*, *21*). The collagen valve had well-separated leaflets, was robust enough to be handled in air (Fig. 4, B and C, and movie S7), and was imaged by micro–computed tomography (μCT) (Fig. 4, D and E, and movie S8). Print fidelity was quantified using gauging to overlay the μCT data on the 3D model (fig. S13B), showing average overprinting of +0.55 mm and underprinting of −0.80 mm (Fig. 4F and fig. S13, C and D). Mechanical function was demonstrated by mounting the valve in a flow system with a pulsatile pump to simulate physiologic pressures, and we observed cyclical opening and closing of the valve leaflets (Fig. 4G and movie S7). We quantified flow through the valves (Fig. 4H) and demonstrated <15% regurgitation (Fig. 4I) with a maximum area opening of 19.5% (Fig. 4G). Additionally, the maximum transvalvular pressure was greater than 40 mmHg for the collagen and alginate valves (Fig. 4J), exceeding standard physiologic pressures for the tricuspid and pulmonary valves but less than the aortic and mitral valves (*22*). Further, human umbilical vein endothelial cells (HUVECs) cultured on unfixed collagen leaflets formed a confluent monolayer (fig. S13E).

A magnetic resonance imaging (MRI)–derived computer-aided design (CAD) model of an adult human heart was created, complete with internal structures such as valves, trabeculae, large veins, and arteries, but lacking smaller-scale vessels. To address this, we developed a computational method that uses the coronary arteries as the template to generate multiscale vasculature (fig. S14 and movie S9). We created a space-filling branching network based on a 3D Voronoi lattice, where vessels further from the left coronary arteries (red to blue) have a denser network and smaller diameters, down to ~100 μm (Fig. 4K). A subregion of the generated vasculature containing the left anterior descending artery (LAD) was selected, rendered, and printed from collagen at adult human scale (Fig. 4, L to N). Patency of large vessels was demonstrated by perfusing the multiscale vasculature through the root of the LAD (Fig. 4O). We confirmed the patency of vessels ~100 μm in diameter by optically clearing and reperfusing the multiscale vasculature (Fig. 4P, fig. S14, N to P, and movie S9).

Finally, to demonstrate organ-scale FRESH v2.0 printing capabilities and the potential to engineer larger scaffolds, we printed a neonatal-scale human heart from collagen (Fig. 4, Q and R, and fig. S15, A to C). To highlight the microscale internal structure, we printed half the heart (Fig. 4S). Structures such as trabeculae were printed from collagen with the same architecture as defined in the G-code file (Fig. 4, T and U). The square-lattice infill pattern within the ventricular walls was similarly well defined (Fig. 4, V and W). We used μCT imaging to confirm reproduction of all the anatomical structures contained within the 3D model of the heart, including the atrial and ventricular chambers, trabeculae, and pulmonary and aortic valves (fig. S15, D to I, and movie S10).

We have used the human heart for proof of concept; however, FRESH v2.0 printing of collagen is a platform that can build advanced tissue scaffolds for a wide range of organ systems. There are still many challenges to overcome, such as generating the billions of cells required to 3D-bioprint large tissues, achieving manufacturing scale, and creating a regulatory process for clinical translation (*23*). Although the 3D bioprinting of a fully functional organ is yet to be achieved, we now have the ability to build constructs that start to recapitulate the structural, mechanical, and biological properties of native tissues.

REFERENCES AND NOTES

1. J. U. Lind *et al.*, *Nat. Mater.* **16**, 303–308 (2017).
2. X. Ma *et al.*, *Proc. Natl. Acad. Sci. U.S.A.* **113**, 2206–2211 (2016).
3. B. Grigoryan *et al.*, *Science* **364**, 458–464 (2019).
4. J. S. Miller *et al.*, *Nat. Mater.* **11**, 768–774 (2012).
5. D. B. Kolesky, K. A. Homan, M. A. Skylar-Scott, J. A. Lewis, *Proc. Natl. Acad. Sci. U.S.A.* **113**, 3179–3184 (2016).
6. H.-W. Kang *et al.*, *Nat. Biotechnol.* **34**, 312–319 (2016).
7. T. J. Hinton, A. Lee, A. W. Feinberg, *Curr. Opin. Biomed. Eng.* **1**, 31–37 (2017).
8. N. Noor *et al.*, *Adv. Sci.* **6**, 1900344 (2019).
9. C. Frantz, K. M. Stewart, V. M. Weaver, *J. Cell Sci.* **123**, 4195–4200 (2010).
10. K. E. Drzewiecki *et al.*, *Langmuir* **30**, 11204–11211 (2014).
11. N. Diamantides *et al.*, *Biofabrication* **9**, 034102 (2017).
12. S. Rhee, J. L. Puetzer, B. N. Mason, C. A. Reinhart-King, L. J. Bonassar, *ACS Biomater. Sci. Eng.* **2**, 1800–1805 (2016).
13. B. Duan, E. Kapetanovic, L. A. Hockaday, J. T. Butcher, *Acta Biomater.* **10**, 1836–1846 (2014).
14. K. Pusch, T. J. Hinton, A. W. Feinberg, *HardwareX* **3**, 49–61 (2018).
15. See supplementary materials.
16. T. J. Hinton *et al.*, *Sci. Adv.* **1**, e1500758 (2015).
17. M. Potente, H. Gerhardt, P. Carmeliet, *Cell* **146**, 873–887 (2011).
18. L. R. Madden *et al.*, *Proc. Natl. Acad. Sci. U.S.A.* **107**, 15211–15216 (2010).
19. A.-K. Olsson, A. Dimberg, J. Kreuger, L. Claesson-Welsh, *Nat. Rev. Mol. Cell Biol.* **7**, 359–371 (2006).
20. B. Duan, L. A. Hockaday, K. H. Kang, J. T. Butcher 3rd, *J. Biomed. Mater. Res. A* **101**, 1255–1264 (2013).
21. H.-G. Lim, G. B. Kim, S. Jeong, Y. J. Kim, *Eur. J. Cardiothorac. Surg.* **48**, 104–113 (2015).
22. A. Hasan *et al.*, *J. Biomech.* **47**, 1949–1963 (2014).
23. J. S. Miller, *PLOS Biol.* **12**, e1001882 (2014).

ACKNOWLEDGMENTS

We thank D. Trumble and K. Cook for access to and assistance with pulsatile flow setup, Doppler flow velocimetry, and pressure transducer measurements; Y. L. Wang for use of the Form 2 3D printer; S. Sohn for time-lapse imaging of the "CMU" print; and K. Verdelis for assistance with μCT analysis. **Funding:** Supported by NIH grants DP2HL117750, F32HL142229, and R21HD090679, FDA grant R01FD006582, NSF grant CMMI 1454248, Office of Naval Research grant N00014-17-1-2566, Congressional Directed Medical Research Program grant W81XWH1610018, and the College of Engineering at Carnegie Mellon University under the Bioengineered Organs Initiative and the Manufacturing Futures Initiative. **Author contributions:** A.L., A.R.H., T.J.H., D.J.S., J.W.T., S.Y., J.M.B., and A.W.F. designed the overall experimental plan; A.L., A.R.H., and T.J.H. developed FRESH v2.0 support material and performed validation experiments; S.Y., J.W.T., and D.J.S. designed experiments and performed FRESH printing and in vivo testing of collagen constructs; A.L., J.M.B., D.J.S., and J.W.T. designed experiments, developed hardware and software, and performed FRESH printing and culture of vascular constructs and ventricles; A.R.H. and T.J.H. designed experiments, developed hardware and software, and performed organ-scale FRESH printing of whole heart, multiscale perfusable vasculature, and tri-leaflet heart valve; and A.L., A.R.H., T.J.H., D.J.S., J.W.T., S.Y., J.M.B., P.G.C., and A.W.F. interpreted data and wrote the manuscript. **Competing interests:** A.L., A.R.H., T.J.H., and A.W.F. all have an equity stake in FluidForm Inc., which is a startup company commercializing FRESH 3D printing. FRESH 3D printing is the subject of patent protection including U.S. Patent 10,150,258 and others. A.W.F. has an equity stake in Biolife4D Inc. and is a member of its scientific advisory board. **Data and materials availability:** All data are available in the main text and the supplementary materials. FRESH v2.0 support material is available from A.W.F. under a material agreement with Carnegie Mellon University. The STL files for 3D bioprinter hardware modifications, collagen constructs, and perfusion systems are available under an open-source CC-BY-SA license at https://3dprint.nih.gov/users/awfeinberg.

SUPPLEMENTARY MATERIALS

science.sciencemag.org/content/365/6452/482/suppl/DC1
Materials and Methods
Figs. S1 to S15
Table S1
Movies S1 to S10
References (*24*–*27*)

3 November 2018; accepted 5 June 2019
10.1126/science.aav9051

3D bioprinting of collagen to rebuild components of the human heart

A. Lee, A. R. Hudson, D. J. Shiwarski, J. W. Tashman, T. J. Hinton, S. Yerneni, J. M. Bliley, P. G. Campbell and A. W. Feinberg

Science **365** (6452), 482-487.
DOI: 10.1126/science.aav9051

If I only had a heart

3D bioprinting is still a fairly new technique that has been limited in terms of resolution and by the materials that can be printed. Lee *et al.* describe a 3D printing technique to build complex collagen scaffolds for engineering biological tissues (see the Perspective by Dasgupta and Black). Collagen gelation was controlled by modulation of pH and could provide up to 10-micrometer resolution on printing. Cells could be embedded in the collagen or pores could be introduced into the scaffold via embedding of gelatin spheres. The authors demonstrated successful 3D printing of five components of the human heart spanning capillary to full-organ scale, which they validated for tissue and organ function.

Science, this issue p. 482; see also p. 446